Environmental Science and Pollution Research (2022) 29:35204–35216
https://doi.org/10.1007/s11356-021-18042-9

RESEARCH ARTICLE

Synthesis of magnetic nanocomposite Fe_3O_4@ZIF-8@ZIF-67 and removal of tetracycline in water

Xu Song[1] · Jingqian Mo[1] · Yuting Fang[1] · Shumin Luo[1] · Jingjing Xu[1] · Xu Wang[1]

Received: 16 July 2021 / Accepted: 7 December 2021 / Published online: 20 January 2022

Abstract

We prepared a double-layer magnetic nanocomposite Fe_3O_4@ZIF-8@ZIF-67 by layer-by-layer self-assembly. Fe_3O_4@ZIF-8@ZIF-67 was used to remove tetracycline from an aqueous solution via a combination of adsorption and Fenton-like oxidation. Depending on the outstanding porous structure of the Fe_3O_4@ZIF-8@ZIF-67, a high adsorption capacity for tetracycline was 356.25 mg g^{-1}, with > 95.47% removal efficiency within 100 min based on Fenton-like oxidation. To better understand the mechanisms involved in integrated adsorption and Fenton-like oxidation, various advanced characterization techniques were used to monitor the changes in morphology and composition of Fe_3O_4@ZIF-8@ZIF-67 before and after removal of tetracycline. Scanning electron microscopy/energy-dispersive X-ray spectroscopy (SEM/EDS), Fourier transform infrared spectroscopy (FTIR), and X-ray diffraction (XRD) all supported adsorption and Fenton oxidation of tetracycline. This study extends the application of Fe_3O_4@ZIF-8@ZIF-67 for environmental remediation.

Keywords Fe_3O_4@ZIF-8@ZIF-67 · Tetracycline · Adsorption · Fenton-like oxidation · H_2O_2

Introduction

Antibiotic consumption has increased globally from usage in human and animal disease treatment, growth promotion, and prophylaxis (Kovalakova et al. 2020). Most ingested antibiotics are released into the aquatic environment instead of being metabolized by organisms (Kraemer et al. 2019). Tetracycline (TC), which ranks second in terms of global production and usage, was discovered in the 1940s (Jeong et al. 2010). Recent results suggest that the concentration of TC in the surface water is ~ 0.15 ug/L (Guo et al. 2017). Environmental TC residues may destroy ecosystems and result in the development of antibiotic-resistant bacteria (ARB) (Wang et al. 2020). Thus, it is critical and urgent to remove TC from the aquatic environment.

Successful TC removal has been achieved by adsorption (Bao et al. 2018), photocatalytic oxidation (Wang et al. 2020), electrochemistry (Bao et al. 2018), ozonation (Wang et al. 2011), Fenton and Fenton-like oxidation (Kong et al. 2020), and biodegradation (Shao et al. 2019). However, the development of these methods has been confined because of their disadvantages, such as a poor adsorption performance, low visible-light response, high energy consumption, complicated equipment, and harsh reaction conditions (Wang et al. 2011, 2020; Bao et al. 2018; Shao et al. 2019; Kong et al. 2020; Zhao et al. 2020). A combined process may overcome these limitations by integrating two or more strategies, such as the combination of adsorption and microbial metabolism (Zhao et al. 2020), adsorption and photocatalytic oxidation (Wang et al. 2019), electrochemistry and photocatalytic oxidation (Liu et al. 2009), and photocatalytic and Fenton oxidation (Han et al. 2020). In contrast, the combination of adsorption and Fenton-like oxidation is environmentally friendly, efficient, and operationally straightforward (Weng et al. 2020). Therefore, it is critical to source a material that can achieve adsorption and Fenton-like oxidation.

Metal–organic frameworks (MOFs), which are a type of porous coordination polymer, are comprised of metal ions or clusters that are coordinated to organic linkers (Cook et al. 2013; Tibbetts and Kostakis 2020). The past three

Responsible Editor: Santiago V. Luis

✉ Jingjing Xu
jjyf18@163.com

✉ Xu Wang
wangxu@hmc.edu.cn

[1] School Laboratory Medicine, Hangzhou Medical College, Hangzhou 310058, Zhejiang, People's Republic of China

decades have witnessed enormous growth in MOF research from synthesis to uses in adsorption, storage, separation, and catalysis (Stock and Biswas 2012). Numerous previous studies have shown that MOFs have an excellent effect on TC removal from wastewater with their large surface areas and high porosity (Li et al. 2020a; Xiao et al. 2020). To date, most studies have focused on the use of MOFs as an adsorbent, and little information is available on the performance and mechanism of TC removal from wastewater via synergetic adsorption and Fenton-like oxidation using magnetic MOFs.

In this study, a double-layer magnetic MOF (Fe_3O_4@ZIF-8@ZIF-67) was prepared by a solvothermal method in layer-by-layer self-assembly. The structure of the double layer could expand the porosity and specific surface area for adsorption and provide more active sites for Fenton-like oxidation. Good magnetic properties could contribute to recycle from the reaction system. The main aim of this study was to discuss TC removal by using Fe_3O_4@ZIF-8@ZIF-67 by synergetic adsorption and Fenton-like oxidation.

Experimental

Reagents

Tetracycline hydrochloride (TC) was purchased from Rhawn Technology Development Co., Ltd. (Shanghai, China). Ethanol and ammonium hydroxide ($NH_3{\cdot}H_2O$, 25–28 wt%) were obtained from Sanying Chemical Reagents Co., Ltd. (Zhejiang, China). $FeSO_4{\cdot}7H_2O$ was supplied by Qiangsheng Functional Chemical Co., Ltd. (Jiangsu, China). $FeCl_3{\cdot}6H_2O$ and tertiary butanol were purchased from Sinopharm Chemical Reagents Co., Ltd. (Shanghai, China). Hydrochloric acid (36–38 wt%) and $Zn(NO_3)_2{\cdot}6H_2O$ were obtained from Lingfeng Chemical Reagents Co., Ltd. (Shanghai, China). Nanometer iron powder (99% metals basis, 50 nm) was obtained from Chaowei Nano Technology Co., Ltd. (Shanghai, China). Activated carbon (mesh ≥ 200), humid acid (HA, fulvic acid ≥ 90%), 2-methylimidazole ($C_4H_6N_2$), methyl alcohol (CH_3OH), and $Co(NO_3)_2{\cdot}6H_2O$ were obtained from Aladdin Reagent Inc. (Shanghai, China). All reagents were used as received without further purification.

Synthesis of Fe_3O_4 NPs

Fe_3O_4 nanoparticles (NPs) were prepared by a modified coprecipitation method based on a previous study (Li et al. 2020b). They were synthesized as follows. $FeCl_3{\cdot}6H_2O$ (1.35 g) and $FeSO_4{\cdot}7H_2O$ (0.695 g) were dissolved in distilled water (100 mL). Nitrogen gas was injected. The mixture was heated to 70℃ under vigorous stirring until a turbid solution formed. Heating was continued for 25 min. $NH_3{\cdot}H_2O$ (5 mL) was added to the mixture, and the solution was stirred at 80℃ for 30 min. The mixture was cooled to room temperature. The solid was separated from the solution by magnetic separation and washed several times with deionized water.

Synthesis of Fe_3O_4@ZIF-8@ZIF-67

Fe_3O_4@ZIF-8@ZIF-67 was prepared by using a facile solvothermal process. $Zn(NO_3)_2{\cdot}6H_2O$ (2.98 g) was dissolved in CH_3OH (35 mL) to form a solution. Fe_3O_4 and the solution were mixed under ultrasound for 15 min, followed by the addition of a methanol solution (20 mL) of 2-methylimidazole (6.57 g) under ultrasound for 30 min. A methanol solution (15 mL) of $Co(NO_3)_2{\cdot}6H_2O$ (2.91 g) was added to the abovementioned solution, and the ultrasound was maintained for 30 min. The product was collected with an external magnet, washed twice with methanol, and dried at 70℃ for 6 h.

Characterization

Microstructures of the nanocomposite were examined by scanning electron microscopy (SEM, Zeiss Sigma 300, Germany) and X-ray energy-dispersive spectrometry (EDS, BRUKER Quantax EDS with XFlash6 detector, Germany). The nanocomposite crystal structure was detected by X-ray diffraction (XRD, BRUKER D8 Advance, Germany). The infrared spectrum was measured by Fourier transform infrared spectroscopy (FTIR, Nicolet iS5, America). The magnetic properties of the prepared nanoparticles were measured on a vibrating samples magnetometer (VSM, LakeShore 7410, USA). The N_2 adsorption–desorption isotherms were recorded on a fully automatic gas adsorption analyzer (BET, Micromeritics, ASAP 2460 3.00, USA) with a degassing temperature of 120℃ for 8 h, and the adsorption parameters of samples were obtained by Brunauer–Emmett–Teller method.

Batch experiments

Batch removal experiments were conducted in 150-mL conical flasks containing 50 mL of an aqueous sample of TC with a temperature of 25℃ (the influence of temperature was disregarded) and performed on a 150-rpm shaker for 100 min. If necessary, the pH was adjusted with HCl or NaOH (0.1 M).

For the TC adsorption experiments, the effects of the initial concentration, Fe_3O_4@ZIF-8@ZIF-67 dosages (5–40 mg), temperature (25℃, 35℃, and 45℃), initial pH (3–11), and humic acid on TC adsorption were investigated. In a typical process, Fe_3O_4@ZIF-8@ZIF-67 (20 mg) was

added into a 50 mL TC solution (160 mg/L) and shaken for 100 min at 25℃.

All Fenton-like oxidation degradation tests were performed under Fe_3O_4@ZIF-8@ZIF-67 and H_2O_2 system. In a typical process, Fe_3O_4@ZIF-8@ZIF-67 (20 mg) was dispersed in a 50 mL solution of TC (160 mg/L) and H_2O_2 (30 mmol/L) at a certain pH. The influences of Fe_3O_4@ZIF-8@ZIF-67 dosages (5–40 mg), initial pH (3–11), and the concentration of H_2O_2 (0–40 mmol/L) on TC degradation were investigated. To show the quenching of hydroxyl radicals (·OH), tert-butanol was used as a ·OH scavenger. The dosage of tert-butanol was 0 mM, 10 mM, 20 mM, 40 mM, and 60 mM.

When the experiment was completed, the adsorbent was separated from the solution by an external magnet, and the solution was filtered through a 0.22-μm microporous membrane to obtain the supernatant. The concentration of TC was determined by ultraviolet–visible spectrophotometry at 355 nm. The TC concentration was calculated from a standard curve. The removal efficiency *Re* (%) was calculated from (1):

$$R_e = \frac{C_0 - C_t}{C_0} \times 100\% \quad (1)$$

The adsorption capacity (q_t) of TC at any time was calculated using (2):

$$q_t = \frac{(C_0 - C_t)V}{M} \quad (2)$$

where C_0 (mg/L) is the initial concentration of TC, C_t (mg/L) is the concentration of TC at time t (min), V (mL) is the volume of the TC solution, and M (mg) is the adsorbent dosage.

Results and discussion

Characterization

SEM was carried out to observe the morphological of Fe_3O_4, Fe_3O_4@ZIF-8, ZIF-8@ZIF-67, and Fe_3O_4@ZIF-8@ZIF-67, and the changes after adsorption and Fenton-like oxidation of Fe_3O_4@ZIF-8@ZIF-67. SEM micrographs (Fig. 1b) show that Fe_3O_4@ZIF-8 exhibited uniform rhombic dodecahedral shape crystals and was not undermined by Fe_3O_4 NP loading (Sajjadi et al. 2018). Figure 1c and d shows that the material nanostructure of ZIF-8@ZIF-67 and Fe_3O_4@ZIF-8@ZIF-67 changed from a granular to a rod-shaped morphology with the introduction of ZIF-67. Fe_3O_4 NPs were distributed on the surface and inside the ZIF-8@ZIF-67. After adsorption, the morphology of Fe_3O_4@ZIF-8@ZIF-67 was similar to that of the as-prepared one (Fig. 1e), but the particle surface became a little rougher, which is attributed to TC

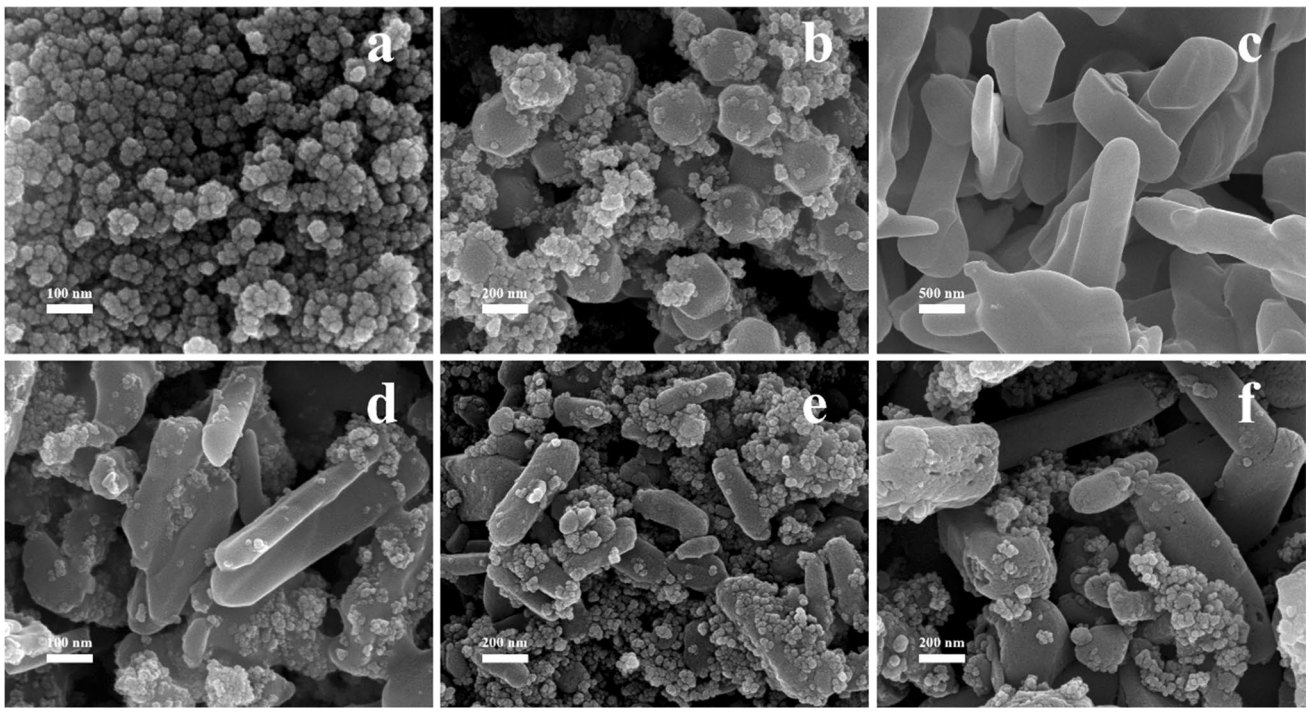

Fig. 1 SEM image of Fe_3O_4 (**a**), Fe_3O_4@ZIF-8 (**b**), ZIF-8@ZIF-67 (**c**), Fe_3O_4@ZIF-8@ZIF-67 before (**d**) and after (**e**) adsorption and after Fenton-like oxidation (**f**)

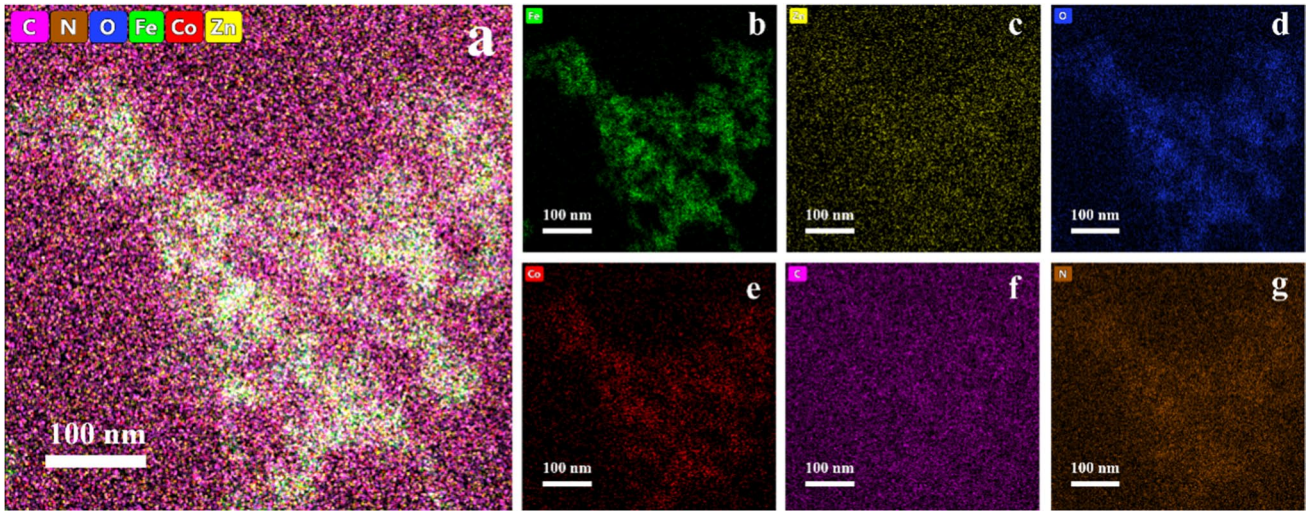

Fig. 2 EDS element mapping of Fe_3O_4@ZIF-8@ZIF-67

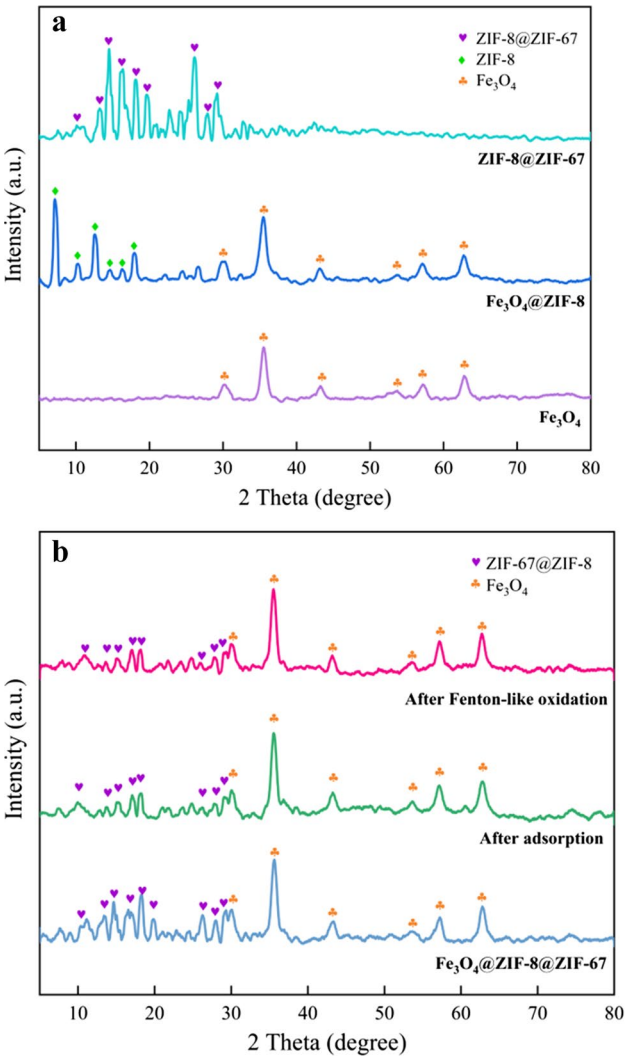

Fig. 3 XRD patterns of Fe_3O_4, Fe_3O_4@ZIF-8, and ZIF-8@ZIF-67 (**a**), and Fe_3O_4@ZIF-8@ZIF-67 before and after adsorption and Fenton-like oxidation (**b**)

adsorption on the Fe_3O_4@ZIF-8@ZIF-67 surface. After Fenton-like oxidation, the morphology of Fe_3O_4@ZIF-8@ZIF-67 was not changed obviously (Fig. 1f) but showed several pinholes and folds. This appearance most likely resulted because the generated OH acted on the structure.

EDS element mapping was used to investigate the elemental distribution of Fe_3O_4@ZIF-8@ZIF-67. Figure 2 shows that C, N, Zn, and Co elements are uniformly distributed in the shell layer, while Fe and O elements are mainly dispersed in the core section of the composite. The mapping of C, N, Zn, and Co elements can be attributed to ZIFs, and the presence of Fe and O can be ascribed to Fe_3O_4. The fact that C, N, O, Fe, Zn, and Co elements are all detected confirmed the successful preparation of Fe_3O_4@ZIF-8@ZIF-67 nanocomposites.

To determine the chemical structure, Fe_3O_4, Fe_3O_4@ZIF-8, ZIF-8@ZIF-67, and Fe_3O_4@ZIF-8@ZIF-67 were analyzed by XRD. The XRD pattern for Fe_3O_4@ZIF-8@ZIF-67 and ZIF-8@ZIF-67 (Fig. 3a and b) had the sane characteristic peaks located at ~ 10.1°, 13.2°, 14.5°, 16.4°, 18.1°, 19.6°, 26.1°, 27.9°, and 29.2°, which agrees with the results in the literature (Li et al. 2020b). The characteristic peaks of Fe_3O_4 were located at 30.0°, 35.6°, 43.4°, 53.7°, 57.2°, and 62.8°, which agreed well with magnetite (JCPDS NO. 19–0629), indicating the successful loading of Fe_3O_4 (Jiang et al. 2016). The introduction of Fe_3O_4 NPs did not destroy the crystallinity of ZIF-8 or ZIF-67, which confirms that Fe_3O_4@ZIF-8@ZIF-67 was synthesized. To verify the crystalline structure stability, the XRD patterns of Fe_3O_4@ZIF-8@ZIF-67 after adsorption and Fenton-like oxidation (Fig. 3b) were analyzed. In Fig. 3b, the peak position and intensity appointed to Fe_3O_4 remained consistent before and after adsorption and Fenton-like oxidation, which shows that the Fe_3O_4 structure was stable. After batch reactions

and Fenton-like oxidation, the magnetic property of Fe_3O_4 remained unchanged and met the practical application of repeated and strong separation. However, after adsorption and Fenton-like oxidation, the diffraction peak intensities indexed to ZIF-8@ZIF-67 decreased compared with that observed prior to reaction, which may be attributed to TC adsorption, which resulted in clogged pores of Fe_3O_4@ZIF-8@ZIF-67 and changes in the nanoparticle surface (Li et al. 2019a). The crystal form and structure of the Fe_3O_4@ZIF-8@ZIF-67 did not show changes because of the existence of characteristic peaks. These results agree with the SEM observations (Fig. 1).

FTIR analysis was carried out to prove the synthesis of Fe_3O_4@ZIF-8@ZIF-67 and to obtain an improved understanding of the possible reaction mechanisms (Fig. 4). As shown in Fig. 4b, the appearance of a peak at 581 cm^{-1} could be related to Fe–O–Fe vibration, which suggests that Fe_3O_4 NPs was loaded successfully. The peaks at 1136–1306 cm^{-1} are ascribed to imidazole ring vibration, whereas those at 2917–3107 cm^{-1} were assigned to the stretching vibration of the saturated hydrocarbon C–H (CH_3) and unsaturated hydrocarbon C–H of the 2-methylimidazolium. Therefore, the 2-methylimidazolium served as an organic ligand in the nanocomposite. The peak at 425 cm^{-1} was caused by the Zn–N and Co–N stretching vibration, and the peaks at 994–1106 cm^{-1} resulted from C = N in ZIF, which confirms the presence of a ZIF-8 and ZIF-67 structure. These characteristic peaks confirm the synthesis of nanocomposite Fe_3O_4@ZIF-8@ZIF-67 in accordance with the XRD results (Fig. 3). In Fig. 5, after adsorption and Fenton-like oxidation, the 1618 cm^{-1} peak that was associated with the benzene ring broadened indicates that TC was adsorbed on the Fe_3O_4@ZIF-8@ZIF-67. Compared with the original Fe_3O_4@ZIF-8@ZIF-67, the main characteristic peaks exhibited no obvious alterations after adsorption or Fenton-like oxidation; thus, it was inferred that the magnetic nanocomposite structure had not been destroyed.

The hysteresis loop from VSM was used to obtain the magnetic properties of Fe_3O_4, Fe_3O_4@ZIF-8, and Fe_3O_4@ZIF-8@ZIF-67. According to the VSM results in Fig. 5, the saturation magnetization (Ms) values of Fe_3O_4, Fe_3O_4@ZIF-8, and Fe_3O_4@ZIF-8@ZIF-67 were 70.21 emu/g, 37.16 emu/g, and 18.38 emu/g, respectively. The phenomenon that the magnetic intensity decreased shows that ZIF-8 and ZIF-67 were coated successively. The as-prepared nanocomposite still exhibited sufficient magnetic responsibility and could be separated with an external magnetic field to facilitate recycling and reuse. Figure 6 shows that Fe_3O_4@ZIF-8@ZIF-67 started to decompose strongly at 500℃, which indicates its good thermal stability.

The surface area and porosity of Fe_3O_4@ZIF-8@ZIF-67 and Fe_3O_4@ZIF-8 were shown in Supplementary Fig. S1. The BET surface area of Fe_3O_4@ZIF-8 was 346.7 m^2/g, and that of Fe_3O_4@ZIF-8@ZIF-67 was slightly lower (328.7 m^2/g). The isotherms are a combination of type I isotherms, which suggested a typical microporous structure. The detailed porosity results of the two adsorbents were listed in Supplementary Table S1.

Adsorption performance of Fe_3O_4@ZIF-8@ZIF-67

Different factors affect the adsorption process, and the Fe_3O_4@ZIF-8@ZIF-67 dosage, temperature, pH, initial concentration of TC, and HA were investigated by a variable-controlling strategy.

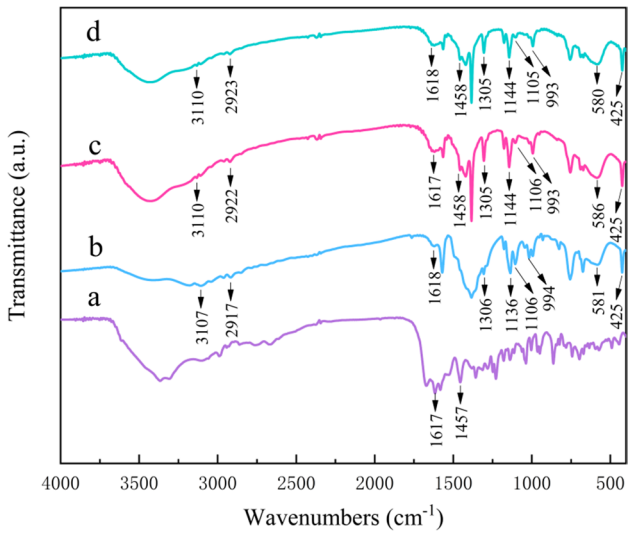

Fig. 4 FTIR spectra of TC (**a**) and Fe_3O_4@ZIF-8@ZIF-67 before (**b**) and after (**c**) adsorption, and after Fenton-like oxidation (**d**)

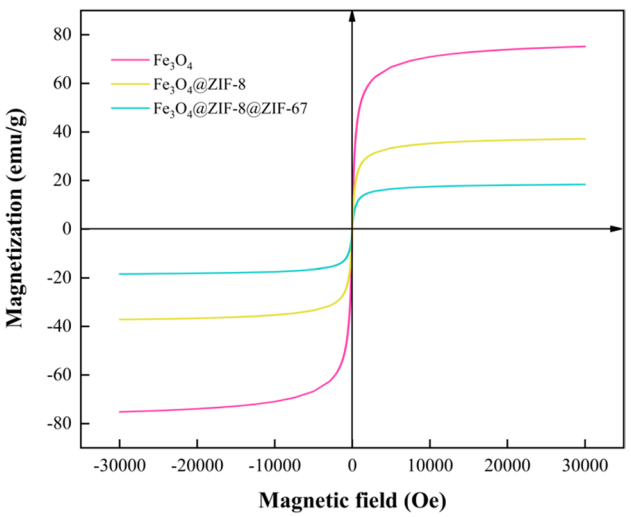

Fig. 5 Hysteresis loop diagram of Fe_3O_4, Fe_3O_4@ZIF-8, and Fe_3O_4@ZIF-8@ZIF-67

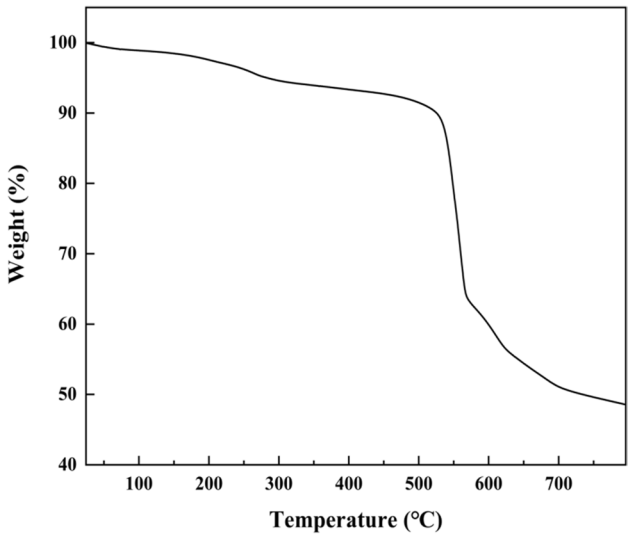

Fig. 6 Thermogravimetric analysis diagram of Fe_3O_4@ZIF-8@ZIF-67

To determine the optimum adsorbent dosage, we explored the adsorbent effect on the TC removal efficiency. As shown in Fig. 7a, with an increase of adsorbent from 5 to 20 mg, the TC removal efficiency improved and reached a maximum removal efficiency of more than 88%. This simply results from sufficient adsorption sites for adsorption. However, the adsorption capacity dropped gradually from 352.88 to 181.00 mg/L when the amount of the adsorbent further increased from 20 to 40 mg. This is because the unsaturated adsorption is caused by the excessive adsorbent, resulting in the decrease in adsorption per unit mass of Fe_3O_4@ZIF-8@ZIF-67, which leads to a decrease in adsorption capacity.

Temperature determines the velocity of the molecular motion and the energy of the molecular surface, which affects the mass transfer rate. Therefore, it is important to study the effect of temperature on the adsorption process. Figure 7b shows that, with an increase in temperature, the adsorption capacity of Fe_3O_4@ZIF-8@ZIF-67 on TC increases slightly, which indicates that the adsorption is an endothermic process. This phenomenon may be attributed to the improved dispersion rate of TC molecules as the temperature increases, and as a result, TC molecules can pass through the external boundary faster.

As the initial concentration of TC increases, the adsorption capacity of TC improves, which shows that the initial concentration of contaminants may affect the mass transfer rate. A higher concentration increases the effective collision probability between the adsorbate and the adsorbent, which causes the adsorption to move in a positive direction. When the initial concentration reaches 120 mg/L, the removal efficiency exceeds 90%. However, there is no further significant change in removal efficiency when the initial concentration continues to increase. This behavior may be related to the saturation of active sites in Fe_3O_4@ZIF-8@ZIF-67, which cannot adsorb total TC at higher concentrations.

We investigated the adsorption quantity of double-layer MOF on TC at different pH. As indicated in Fig. 7c, the removal efficiency of TC exceeded 88% and remained stable for a pH of 5–7. Under strongly acidic (pH 3) or basic (pH 11) conditions, respectively, the adsorption efficiency decreases. This may be due to certain collapse of MOFs structure under acidic (pH 3) conditions (Han et al. 2018). At high ambient pH (pH 11), the amount of deprotonation of phenolic hydroxyl groups of TC increases, which may weaken the adsorption interaction.

It is meaningful to explore the effect of HA on the adsorption of TC because HA exists extensively in natural water and wastewater. Figure 7d shows the variation tendency in adsorption capacity of Fe_3O_4@ZIF-8@ZIF-67 with the concentration of HA range from 0 to 8 mg/L. The adsorption capability of Fe_3O_4@ZIF-8@ZIF-67 hardly changes as the HA concentration increases. This phenomenon shows that Fe_3O_4@ZIF-8@ZIF-67 is an efficient adsorbent in HA-enriched water.

Catalytic performance of Fe_3O_4@ZIF-8@ZIF-67

The removal efficiencies of TC were evaluated using Fe_3O_4@ZIF-8@ZIF-67 and H_2O_2 (Fig. 8). The sole H_2O_2 system induced only 1.31% removal efficiency of TC within 180 min, indicating insignificant self-activated oxidation of H_2O_2. With the introduction of Fe_3O_4@ZIF-8@ZIF-67, 95.76% of TC was removed in Fe_3O_4@ZIF-8@ZIF-67/H_2O_2 system, which was higher than the combined removal efficiency with H_2O_2 (1.31%) and Fe_3O_4@ZIF-8@ZIF-67 (89.03%) alone. These results show that Fe_3O_4@ZIF-8@ZIF-67 could be a favorable catalyst for H_2O_2 activation. The addition of H_2O_2 compensated for the deficiency that Fe_3O_4@ZIF-8@ZIF-67 alone had a weak adsorption efficiency for low concentration of TC, and the TC removal from aqueous solution rose to a new high. Figure 8 (inset) shows that the TC removal efficiency of the Fe_3O_4@ZIF-8@ZIF-67/H_2O_2 system minus the Fe_3O_4@ZIF-8@ZIF-67 system decreased progressively, which indicates that Fenton-like oxidation acted mainly on the TC molecules that were adsorbed on the Fe_3O_4@ZIF-8@ZIF-67 instead of the free TC molecules in an aqueous solution. Therefore, with synergetic adsorption and Fenton-like oxidation, TC molecules were adsorbed preferentially on the Fe_3O_4@ZIF-8@ZIF-67 and, afterwards, some were oxidized by radicals that were generated by H_2O_2. This is similar to the literature report by Hou et al. that an efficient "capture" is crucial for the following "destroy" (Hou et al. 2020).

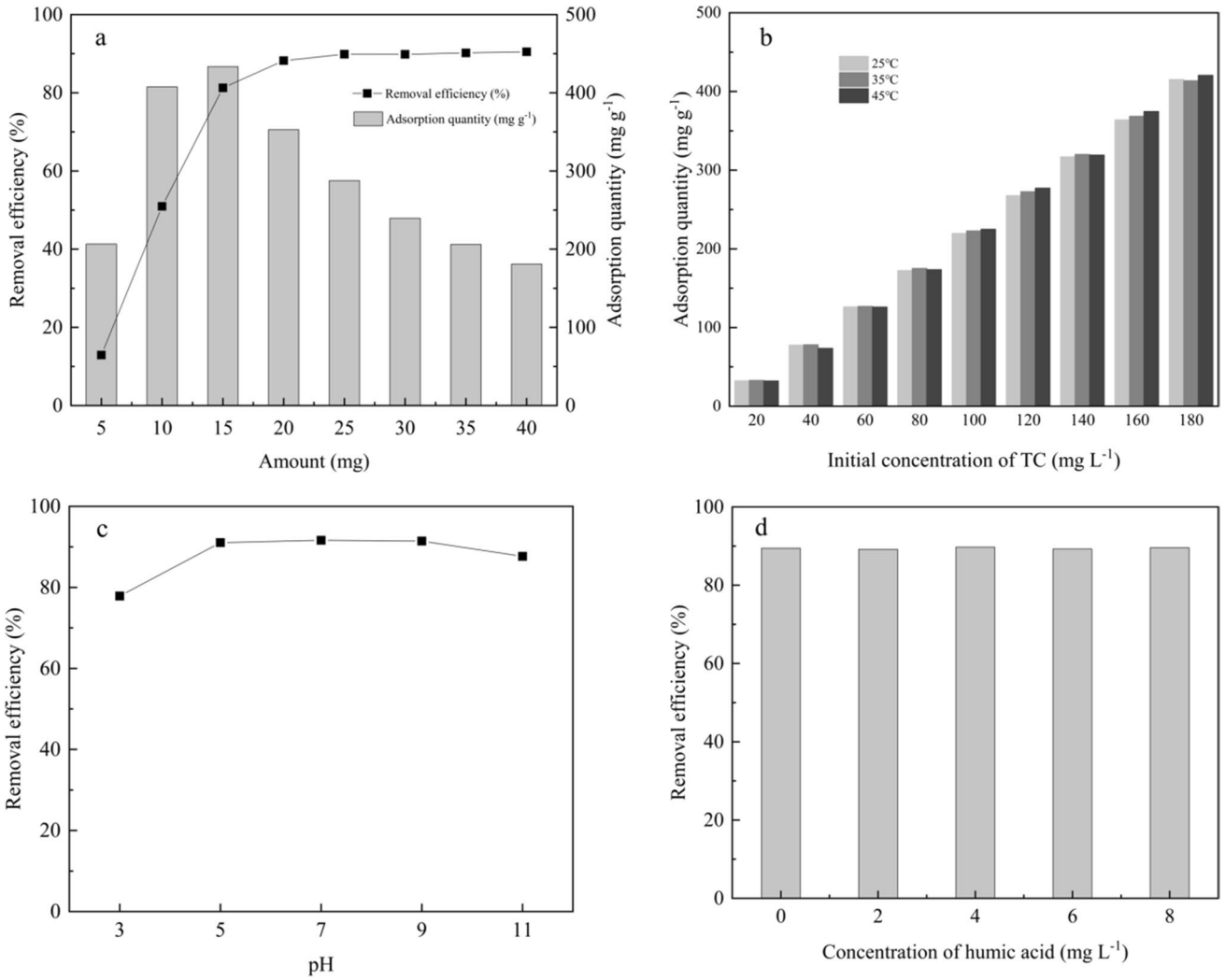

Fig. 7 Treatment parameters of adsorption of TC from Fe_3O_4@ZIF-8@ZIF-67. (**a**) Effect of amount on TC adsorption (conditions: volume = 50 mL; C_0 (TC) = 160 mg/L; T = 25℃; reaction time = 100 min; amount of adsorbent = 5, 10, 15, 20, 25, 30, 35, 40 mg). (**b**) Effect of initial concentration on TC adsorption (conditions: volume = 50 mL; material dose = 0.4 g/L; T = 25℃; reaction time = 100 min; initial concentration = 20, 40, 60, 80, 100, 120, 140, 160, 180 mg/L). (**c**) Effect of pH on TC adsorption (conditions: volume = 50 mL; material dose = 0.4 g/L; T = 25℃; reaction time = 100 min; pH = 3, 5, 7, 9, 11). (**d**) Effect of concentration of humic acid on TC adsorption (conditions: volume = 50 mL; material dose = 0.4 g/L; T = 25℃; reaction time = 100 min; concentration of humic acid = 0, 2, 4, 6, 8 mg/L)

In Fenton-like reactions, the concentration of H_2O_2, the primary pH of the solution, and the adsorbent dosage may influence the oxidation performance, and thus, the effect of the abovementioned conditions on the catalytic oxidation of TC was investigated as follows.

As shown in Fig. 9, TC removal efficiency boosts with increasing Fe_3O_4@ZIF-8@ZIF-67 dosage from 5 to 20 mg, attributable to the increase of availability of active sites and the generation of radicals (Ahmed et al. 2016). The maximum removal efficiency (95.75%) was shown at the dosage of 20 mg. When the amount of the adsorbent further increased, the removal efficiency barely improved. This may be due to the limiting of H_2O_2 concentration and the scavenging effect of excess adsorbent to hydroxyl radicals, which were wildly reported in previous works (Ahmed et al. 2016; Shi et al. 2018).

H_2O_2 can oxidize a variety of organic compounds, such as carboxylic acids, alcohols, and esters, into inorganic states, and thus, it is important in Fenton-like reactions. Therefore, it is necessary to explore the influence of H_2O_2 concentration. As shown in Fig. 10, with increasing H_2O_2 concentration from 0 to 35 mM, the removal efficiency of TC improves from the initial 90.40% to a maximum of 98.97%. During this process, the increased hydroxyl radicals improved the oxidation efficiency. With a further increase of H_2O_2 concentration, the removal efficiency

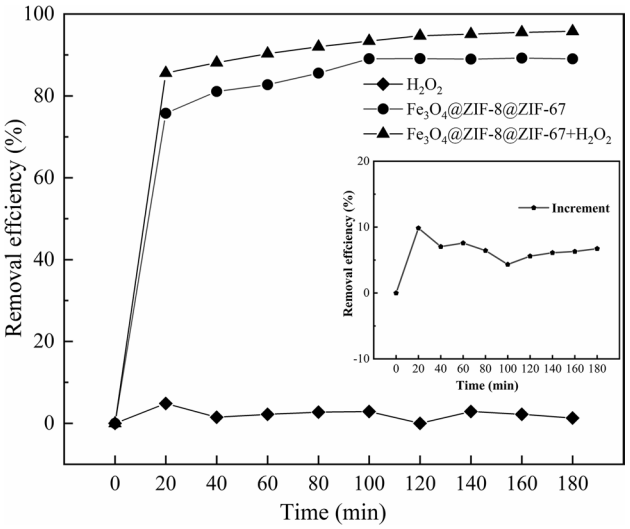

Fig. 8 TC removal efficiency using different catalytic systems and the inset shows the increment of removal efficiency between Fe_3O_4@ZIF-8@ZIF-67/H_2O_2 system and Fe_3O_4@ZIF-8@ZIF-67 system (conditions: volume = 50 mL, material dose = 0.4 g/L, C_0 (TC) = 160 mg/L, C (H_2O_2) = 30 mM, T = 25℃)

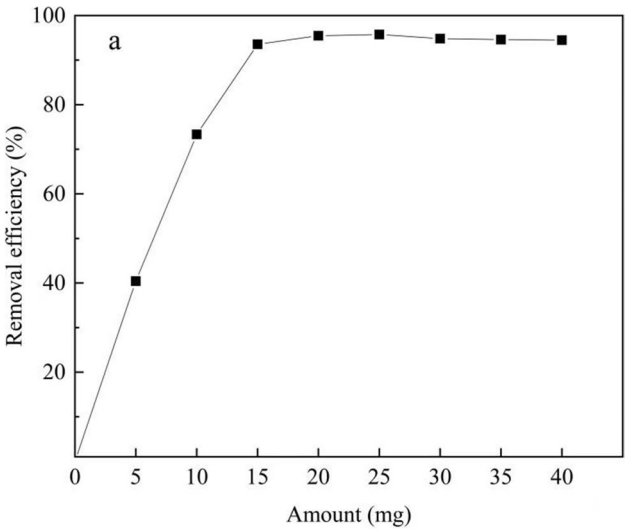

Fig. 9 Effect of amount of Fe_3O_4@ZIF-8@ZIF-67 on TC removal efficiency (conditions: volume = 50 mL, material dose = 5, 10, 15, 20, 25, 30, 35, 40 mg, C_0 (TC) = 160 mg/L, C (H_2O_2) = 30 mM, T = 25℃)

decreased gradually. A reason for the behavior may be ascribed to the self-quenching of radicals (Eq. (3)) and the elimination effect of excessive H_2O_2 to ·OH (Eqs. (4)–(5)) (Shi et al. 2016; Dias et al. 2016):

$$\cdot OH + \cdot OH \rightarrow H_2O_2 \quad (3)$$

$$H_2O_2 + \cdot OH \rightarrow H_2O + HOO\bullet \quad (4)$$

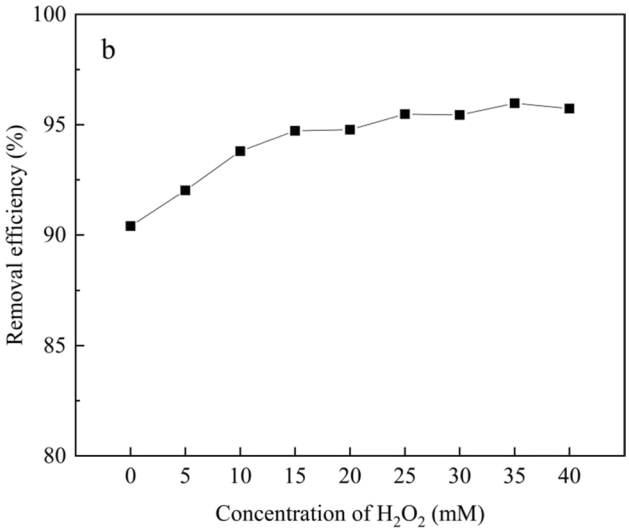

Fig. 10 Effect of initial concentration of H_2O_2 on TC removal efficiency (conditions: volume = 50 mL, material dose = 0.4 g/L, C_0 (TC) = 160 mg/L, T = 25℃)

$$HOO\bullet + \cdot OH \rightarrow H_2O + O_2 \quad (5)$$

pH is an important factor to control the generation of ions and free radicals in Fenton-like reactions. As shown in Fig. 11, when the pH ranges from 3 to 9, the removal efficiency was sustained over 90%, which shows that Fe_3O_4@ZIF-8@ZIF-67/H_2O_2 system has a good TC removal under acid and neutral conditions. When pH was exceeded 9, the removal efficiency drops to 78.69%. This is possibly due to the auto self-decomposition of H_2O_2 to H_2O and O_2, and the rapid conversion of ·OH to its less active conjugate base, $\cdot O^-$, in alkaline conditions (Babuponnusami and Muthukumar 2012). Compared with TC absorption by independent Fe_3O_4@ZIF-8@ZIF-67, the removal efficiency by Fe_3O_4@ZIF-8@ZIF-67/H_2O_2 system increased the most (12.24%) when pH was 3. This is because H_2O_2 was more likely to produce ·OH in an acidic environment to promote oxidation reaction, and the oxidation potential of ·OH is fairly strong in acidic conditions (Burbano et al. 2005). Overall, with the synergistic effect of absorption and oxidation, the Fe_3O_4@ZIF-8@ZIF-67 heterogeneous Fenton system can be used in a wider pH range (pH 3–9) than traditional Fenton-like system and has better environmental adaptability.

Kinetics analysis

TC removal consists of two sections, i.e., adsorption and Fenton-like oxidation. The following explains the two sections:

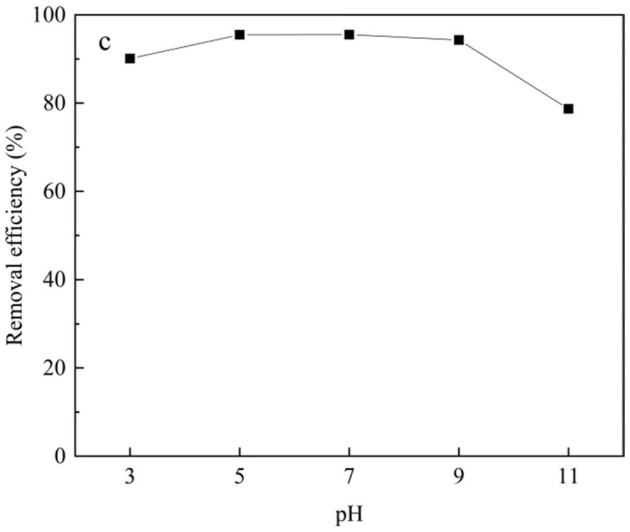

Fig. 11 Effect of pH on TC removal efficiency (conditions: volume = 50 mL, material dose = 0.4 g/L, C_0 (TC) = 160 mg/L, C (H_2O_2) = 30 mM, T = 25℃)

Adsorption kinetics

Adsorption kinetics were described by the pseudo-first-order (Eq. (6)) and pseudo-second-order (Eq. (7)) kinetic models:

$$\ln\left(q_e - q_t\right) = \ln q_e - k_1 t \tag{6}$$

$$\frac{t}{q_t} = \frac{1}{k_2 q^2{}_e} + \frac{t}{q_e} \tag{7}$$

where q_e and q_t (mg/g) are the amounts of TC adsorption at equilibrium and time t (min), respectively, and k_1 (min^{-1}) and k_2 (g/mg/min) are the rate constants for the pseudo-first-order and pseudo-second-order kinetic models, respectively. The best-fit kinetic parameters of TC adsorption are presented in Table 1 at 25℃. The resulting best linear correlation coefficients for the pseudo-second-order kinetic model (R^2 = 0.99788) were greater than those for the pseudo-first-order kinetic model (R^2 = 0.97004) (Table 1), which shows that the adsorption process followed the pseudo-second-order kinetic model at 25℃ and chemisorption was dominant in the speed limit.

Table 1 Best-fit kinetics parameters for TC adsorption by Fe_3O_4@ZIF-8@ZIF-67

Reaction temperature (℃)	Pseudo-first-order kinetic model		Pseudo-second-order kinetic model	
	k_1 (min^{-1})	R^2	k_2 (g/mg/min)	R^2
25	65.9845	0.97004	6.11182×10^{-4}	0.99788

Oxidation kinetics

To explore the TC removal process, data of the Fenton-like oxidation fitted the pseudo-first-order (Eq. (8)) and pseudo-second-order (Eq. (9)) kinetic models:

$$\ln\frac{c_t}{C_0} = -k_{obs} t \tag{8}$$

$$\ln\left(\frac{1}{C_t} - \frac{1}{C_0}\right) = kt \tag{9}$$

where C_0 is the initial concentration of TC and C_t (mg/L) is the concentration of TC at t min, and k_{obs} (min^{-1}) and k (g/mg/min) are the rate constants for the pseudo-first-order and pseudo-second-order kinetic models, respectively. As shown in Table 2, the correlation coefficients for the pseudo-first-order kinetic model (R^2 = 0.94738) were greater than those for the pseudo-second-order kinetic model (R^2 = 0.93004), which means that the pseudo-first-order kinetic model was more appropriate for oxidation.

Comparison of various materials

The double-layer magnetic MOF (Fe_3O_4@ZIF-8@ZIF-67) was compared with the single-layer magnetic MOF (Fe_3O_4@ZIF-8) and other common adsorbents (AC and nZVI) to reflect the adsorption performance. Figure 12 shows that the adsorption efficiency of Fe_3O_4@ZIF-8@ZIF-67 (90.01%) was two or more times that of Fe_3O_4@ZIF-8 (38.47%), which is attributed primarily to the high porosity and larger specific surface area of the former, which results from the double-layer structure. In contrast with AC (68.53%) and nZVI (18.01%), Fe_3O_4@ZIF-8@ZIF-67 showed an exceedingly good adsorption efficiency. The above results indicate that Fe_3O_4@ZIF-8@ZIF-67 was an outstanding TC adsorbent.

A comparison of the synergetic adsorption and Fenton-like oxidation of TC by various materials is shown in Fig. 13. For the two classical Fenton reagents, Fe (nZVI) and Fe^{2+} ($FeSO_4 \cdot 7H_2O$), as high as 82.70% and 84.50% TC could be removed in 100 min, respectively, which depended on ·OH radical generation. By comparison, Fe_3O_4@ZIF-8@ZIF-67 (95.47%) exhibited a superior removal performance compared with the conventional Fenton reagents. After the

Table 2 Best-fit kinetics parameters for TC oxidation

Reaction temperature (℃)	Pseudo-first-order kinetic model		Pseudo-second-order kinetic model	
	k_1 (min^{-1})	R^2	k_2 (g/mg/min)	R^2
25	0.08357	0.94738	0.17699	0.92126

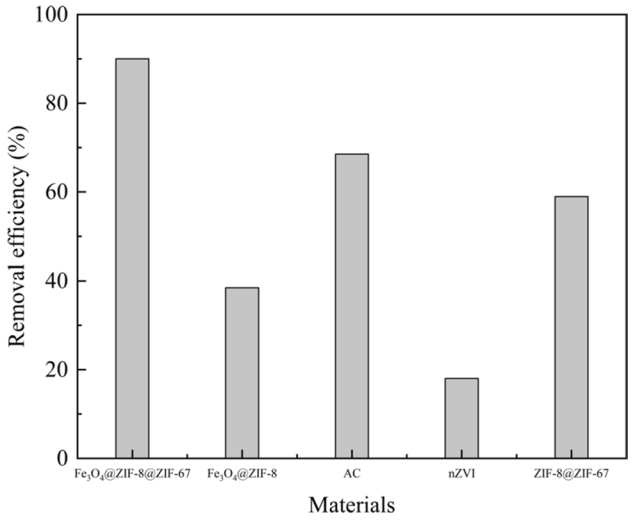

Fig. 12 Effect of various materials on TC adsorption (conditions: volume = 50 mL, material dose = 0.4 g/L, C_0 (TC) = 160 mg/L, T = 25℃, reaction time = 100 min)

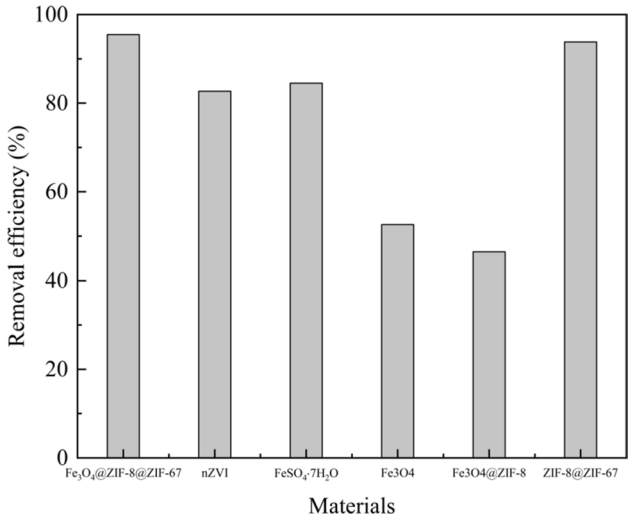

Fig. 13 Effect of various materials on synergetic adsorption and Fenton-like oxidation of TC with the existence of H_2O_2 (conditions: volume = 50 mL, material dose = 0.4 g/L, C_0 (TC) = 160 mg/L, T = 25℃, concentration of H_2O_2 = 30 mM, reaction time = 100 min)

reaction, nZVI decreased because of oxidative degradation and transformed into Fe^{2+}/Fe^{3+}, such as $FeSO_4{\cdot}7H_2O$, which remained in solution and yielded difficulties in separation and recycling (Guo et al. 2020).

In order to investigate the synergetic removal mechanism of Fe_3O_4@ZIF-8@ZIF-67 composite, Fe_3O_4, Fe_3O_4@ZIF-8, and ZIF-8@ZIF-67 were applied to activate H_2O_2 under the same condition. With the existence of H_2O_2, the TC removal efficiency in the Fe_3O_4@ZIF-8 system increased by 7.99%, whereas the ZIF-8@ZIF-67 system (93.81%) showed an increase of 34.85% (Figs. 12 and 13). Fe_3O_4@ZIF-8 and ZIF-8@ZIF-67 all have a similar structure of Zn-ZIFs, which indicates that Co-ZIFs had high catalysis and was the primary active substance. Wu et al. reported a similar finding by using Fe_3O_4@Zn/Co-ZIFs composite to activate PMS for carbamazepine degradation, and they found that Co-ZIFs was the primary active substance (Wu et al. 2020). Zn-ZIFs could not catalyze H_2O_2, but the adsorption was dominated because of the stable valence states of Zn (Wu et al. 2020). The promotion of removal efficiency in the Fe_3O_4@ZIF-8 system resulted mainly from the slight catalysis of Fe_3O_4 NPs that were attached to the ZIF-8 surface (Fig. 13). Overall, Fe_3O_4@ZIF-8@ZIF-67 exhibited a significantly higher removal than other materials in this work.

Removal mechanism

To determine the type of free radicals that were produced during the reaction, free radicals quenching tests were carried out. Tert-butanol (TBA) and ethanol are two commonly used scavengers of free radicals. Ethanol is regarded as scavengers of both $SO_4^{\cdot-}$ and ·OH (Li et al. 2019b), while TBA is considered as the scavenger of only ·OH (Hu et al. 2018). The Fenton-like oxidation reaction mainly catalyzes the H_2O_2 to produce potent oxidative hydroxyl radicals (·OH) to degrade organic pollutants. Therefore, tert-butanol was introduced as a trapping agent to get ·OH. As shown in Fig. 14, with the increase in TBA concentrations (0–60 mM), the TC removal efficiency decreased from 94.48 to 84.99%, which indicates that ·OH played an important role in the degradation of TC. The removal of TC at a high TBA concentration is mainly attributed to the adsorption ability of Fe_3O_4@ZIF-8@ZIF-67. This was similar to the report by Hou et al., where they compared TC removal efficiency by nZVI/MIL-101(Cr) and nZVI/MIL-101(Cr) + H_2O_2 + TBA systems and found both had almost the same TC removal efficiency (Hou et al. 2020).

Based on these results, a proposed pathway and mechanism for Fenton-like oxidation of TC using Fe_3O_4@ZIF-8@ZIF-67 was proposed. This possible mechanism was supported by the obtained characterization (SEM, EDS, XRD, FTIR, VSM, and TG), and kinetics (adsorption and oxidation) data suggested that Fe_3O_4@ZIF-8@ZIF-67 functioned as an adsorbent and a catalyst in the Fenton-like oxidation system. TC molecules were adsorbed rapidly onto the Fe_3O_4@ZIF-8@ZIF-67. The H_2O_2 was activated by Co^{2+} in Fe_3O_4@ZIF-8@ZIF-67 to generate numerous ·OH radicals. TC molecules were oxidized by powerful oxidizing ·OH, degraded into smaller molecules, and even mineralized to H_2O and CO_2 (Hou et al. 2020).

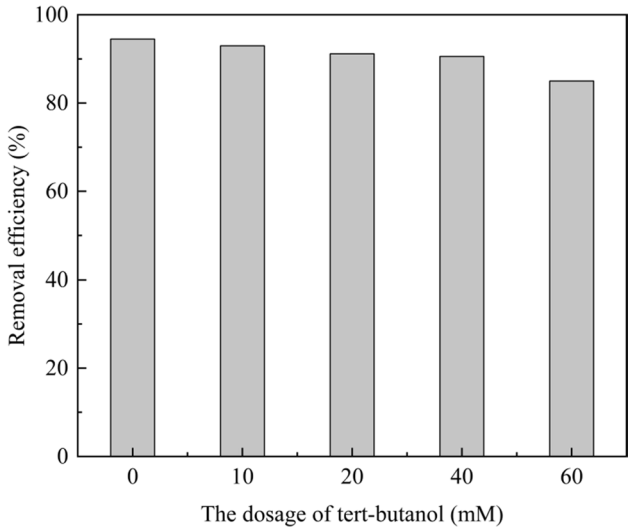

Fig. 14 Effect of dosage of tert-butanol on synergetic adsorption and Fenton-like oxidation of TC (conditions: volume = 50 mL, material dose = 0.4 g/L, C_0 (TC) = 160 mg/L, T = 25℃, reaction time = 100 min)

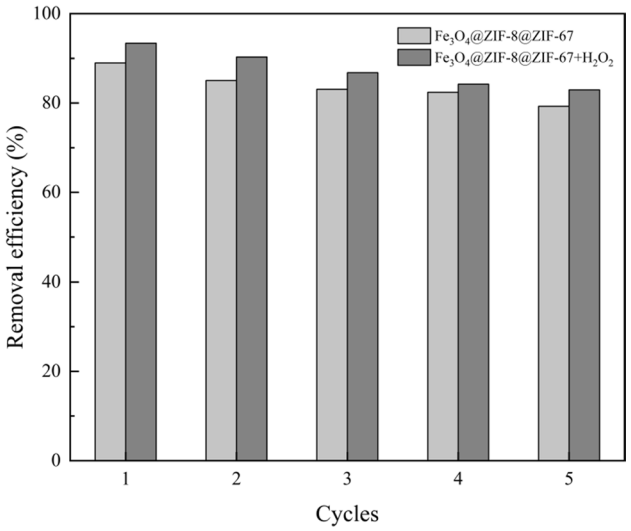

Fig. 15 Reusability of Fe_3O_4@ZIF-8@ZIF-67 in adsorption and Fenton-like oxidation (conditions: volume = 50 mL, material dose = 0.4 g/L, C_0 (TC) = 160 mg/L, T = 25℃, concentration of H_2O_2 = 30 mM, reaction time = 100 min)

Fe_3O_4@ZIF-8@ZIF-67 reusability and stability

For the recycle tests, the Fe_3O_4@ZIF-8@ZIF-67 were separated by magnetism and vortexed with ethanol during adsorption experiments or washed with deionized water during Fenton-like oxidation experiments. After drying at 60℃, the same amount of Fe_3O_4@ZIF-8@ZIF-67 was used for the next recycle with experimental conditions unchanged. Figure 15 shows the reusability of the adsorption and Fenton-like oxidation experiments of Fe_3O_4@ZIF-8@ZIF-67 over five cycles. The removal efficiencies of TC in the adsorption and oxidation experiments decreased to different extents; the removal efficiency in the oxidation experiment was always better than that in the adsorption. The removal efficiencies in the adsorption experiment decreased from 88.96 to 79.27%, and that in the oxidation experiment decreased from 93.38 to 82.94%, which was sufficiently high for practical application. The decrease in removal performance after repeated use may be resulted from the changes in a porous structure that is caused by clearing and washing between the repeated experiments or the absorption of pollutants or byproducts on the active sites of Fe_3O_4@ZIF-8@ZIF-67 (Wu et al. 2020; Zhou et al. 2020).

Moreover, the Co ion leaching in Fe_3O_4@ZIF-8@ZIF-67/H_2O_2 system was also monitored after each cyclic experiment (Supplementary Fig. S2). In the first two cycles, the leached concentration of Co ion was about 0.6 mg/L. In the following three cycles, the leached Co ion increased to 0.8 mg/L with the increase in the number of cycles. The leaching Co ion concentration was below the permissible limit (1 mg/L) according to the Chinese National Standard (GB 25,467–2010). The SEM and FTIR spectroscopy was conducted to further investigate the stability of recovered Fe_3O_4@ZIF-8@ZIF-67 after five runs of Fenton-like oxidation experiments. SEM image (Supplementary Fig. S3) shows that the Fe_3O_4@ZIF-8@ZIF-67 after one cycle was similar to the fresh one. However, after five cycles, the rod-shaped morphology of Fe_3O_4@ZIF-8@ZIF-67 changed and the surface was eroded. After the cycle experiments, the intensity of FTIR peaks assigned to ZIF decrease with respect to Fe_3O_4 (Supplementary Fig. S4). This may be due to the leaching of Co ion, resulting in the reduction of the ZIF ratio in the nanocomposite. In addition, Fe_3O_4@ZIF-8@ZIF-67 was immersed in HCl (pH 3) and NaOH (pH 12) solution to test the acidic and basic stability (Supplementary Fig. S4). The spectra obtained from pH 3 changed obviously in intensity, while those obtained from pH 12 changed a little, which was consistent with previous literature that ZIF has exceptional stability in alkaline water (Park et al. 2006).

Conclusions

The as-prepared magnetic nanocomposite Fe_3O_4@ZIF-8@ZIF-67 is a potential material for TC removal from water in combination with adsorption and Fenton-like oxidation. The adsorption and Fenton-like oxidation experiments indicated that removal efficiency of up to 95.47% was achieved at an initial TC concentration of 160 mg/L, a Fe_3O_4@ZIF-8@ZIF-67 dose of 0.4 g/L, and an H_2O_2 concentration of 30 mM within 100 min at 25℃. Initial kinetic adsorption data best fit a pseudo-second-order kinetic model ($R^2 \geq 0.997$), whereas

the oxidation process best fit a pseudo-first-order model ($R^2 \geq 0.947$). The SEM, EDS, XRD, FTIR, VSM, and TG results confirmed that Fe_3O_4@ZIF-8@ZIF-67 was synthesized and had excellent structural stability and magnetic property. The mechanism is that the high conductivity of Fe_3O_4 NPs promoted Co^{2+} and Co^{3+} cycling. ·OH radicals were generated by H_2O_2 and oxidized the adsorbed TC molecules on the Fe_3O_4@ZIF-8@ZIF-67, which mineralized to H_2O and CO_2. The findings of our study provide theoretical guidance and technical support to treat antibiotics in water by the combined process, and inspiration and a new perspective for morphological design and performance optimization of the new-generation MOFs.

Supplementary Information The online version contains supplementary material available at https://doi.org/10.1007/s11356-021-18042-9.

Author contribution Xu Song: writing—reviewing and editing.
Jingqian Mo: Data curation, writing—original draft preparation.
Yuting Fang: experimental study.
Shumin Luo: experimental study.
Jingjing Xu: oversight and leadership responsibility for the research activity.
Xu Wang: acquisition of the financial support for the project leading to this publication.

Funding This work was supported by the Basic research project of Hangzhou Medical College (KYQN202003) and the Innovation and Entrepreneurship Training Program for College Students (grant no. 202113023011).

Data availability All data generated or analyzed during this study are included in this published article.

Declarations

Ethics approval and consent to participate Not applicable.

Consent for publication Not applicable.

Competing interests The authors declare no competing interests.

References

Ahmed Y, Yaakob Z, Akhtar P (2016) Degradation and mineralization of methylene blue using a heterogeneous photo-Fenton catalyst under visible and solar light irradiation. Catal Sci Technol 6:1222–1232. https://doi.org/10.1039/C5CY01494H

Babuponnusami A, Muthukumar K (2012) Advanced oxidation of phenol: a comparison between Fenton, electro-Fenton, sono-electro-Fenton and photo-electro-Fenton processes. Chem Eng J 183:1–9. https://doi.org/10.1016/j.cej.2011.12.010

Bao J, Zhu Y, Yuan S, Wang F, Tang H, Bao Z, Zhou H, Chen Y (2018) Adsorption of tetracycline with reduced graphene oxide decorated with $MnFe_2O_4$ nanoparticles. Nanoscale Res Lett 13:396

Burbano AA, Dionysiou DD, Suidan MT, Richardson TL (2005) Oxidation kinetics and effect of pH on the degradation of MTBE with Fenton reagent. Water Res 39:107–118. https://doi.org/10.1016/j.watres.2004.09.008

Cook TR, Zheng YR, Stang PJ (2013) Metal-organic frameworks and self-assembled supramolecular coordination complexes: comparing and contrasting the design, synthesis, and functionality of metal-organic materials. Chem Rev 113:734–777

Dias FF, Oliveira AAS, Arcanjo AP, Moura FCC, Pacheco JGA (2016) Residue-based iron catalyst for the degradation of textile dye via heterogeneous photo-Fenton. Appl Catal b: Environ 186:136–142. https://doi.org/10.1016/j.apcatb.2015.12.049

Guo Y, Huang W, Chen B, Zhao Y, Liu D, Sun Y, Gong B (2017) Removal of tetracycline from aqueous solution by MCM-41-zeolite A loaded nano zero valent iron: synthesis, characteristic, adsorption performance and mechanism. J Hazard Mater 339:22–32

Guo B, Xu T, Zhang L, Li S (2020) A heterogeneous Fenton-like system with green iron nanoparticles for the removal of bisphenol A: performance, kinetics and transformation mechanism. J Environ Manage 272:111047

Han C, Zhang C, Tymińska N, Schmidt JR, Sholl DS (2018) Insights into the stability of zeolitic imidazolate frameworks in humid acidic environments from first-principles calculations. J Phys Chem C 122(8):4339–4348. https://doi.org/10.1021/acs.jpcc.7b12058

Han CH, Park HD, Kim SB, Yargeau V, Choi JW, Lee SH, Park JA (2020) Oxidation of tetracycline and oxytetracycline for the photo-Fenton process: their transformation products and toxicity assessment. Water Res 172:115514

Hou X, Shi J, Wang N, Wen Z, Sun M, Qu J, Hu Q (2020) Removal of antibiotic tetracycline by metal-organic framework MIL-101(Cr) loaded nano zero-valent iron. J Mol Liq 313:113512. https://doi.org/10.1016/j.molliq.2020.113512

Hu L, Zhang G, Liu M, Wang Q, Wang P (2018) Enhanced degradation of Bisphenol A (BPA) by peroxymonosulfate with Co_3O_4-Bi_2O_3 catalyst activation: effects of pH, inorganic anions, and water matrix. Chem Eng J 338:300–310. https://doi.org/10.1016/j.cej.2018.01.016

Jeong J, Song W, Cooper WJ, Jung J, Greaves J (2010) Degradation of tetracycline antibiotics: mechanisms and kinetic studies for advanced oxidation/reduction processes. Chemosphere 78:533–540

Jiang H, Sun Y, Feng J, Wang J (2016) Heterogeneous electro-Fenton oxidation of azo dye methyl orange catalyzed by magnetic Fe_3O_4 nanoparticles. Water Sci Technol 74(5):1116–1126. https://doi.org/10.2166/wst.2016.300

Kong Y, Zhuang Y, Shi B (2020) Tetracycline removal by double-metal-crosslinked alginate/graphene hydrogels through an enhanced Fenton reaction. J Hazard Mater 382:121060

Kovalakova P, Cizmas L, McDonald TJ, Marsalek B, Feng M, Sharma VK (2020) Occurrence and toxicity of antibiotics in the aquatic environment: a review. Chemosphere 251:126351

Kraemer SA, Ramachandran A, Perron GG (2019) Antibiotic pollution in the environment: from microbial ecology to public policy. Microorganisms 7:180

Li N, Zhou L, Jin X, Owens G, Chen Z (2019a) Simultaneous removal of tetracycline and oxytetracycline antibiotics from wastewater using a ZIF-8 metal organic-framework. J Hazard Mater 366:563–572

Li Z, Liu D, Zhao Y, Li S, Wei X, Meng F, Huang W, Lei Z (2019b) Singlet oxygen dominated peroxymonosulfate activation by CuO-CeO_2 for organic pollutants degradation: performance and mechanism. Chemosphere 233:549–558. https://doi.org/10.1016/j.chemosphere.2019.05.291

Li K, Li JJ, Zhao N, Ma Y, Di B (2020a) Removal of tetracycline in sewage and dairy products with high-stable MOF. Molecules 25:1312

Li TF, Lu M, Gao YH, Huang XD, Liu GY, Xu DH (2020b) Double layer MOFs M-ZIF-8@ZIF-67: the adsorption capacity and removal mechanism of fipronil and its metabolites from environmental water and cucumber samples. J Adv Res 24:159–166. https://doi.org/10.1016/j.jare.2020.03.013

Liu Y, Gan X, Zhou B, Xiong B, Li J, Dong C, Bai J, Cai W (2009) Photoelectrocatalytic degradation of tetracycline by highly effective TiO_2 nanopore arrays electrode. J Hazard Mater 171:678–683

Park KS, Ni Z, Côté AP, Choi JY, Huang RD, Uribe-Romo FJ, Chae HK, O'Keeffe M, Yaghi OM (2006) Exceptional chemical and thermal stability of zeolitic imidazolate frameworks. P Nati Acad Sci USA 103(27):10186–10191. https://doi.org/10.1073/pnas.0602439103

Sajjadi S, Khataee A, Soltani RDC, Bagheri N, Karimi A, Azar AEF (2018) Implementation of magnetic Fe_3O_4@ZIF-8 nanocomposite to activate sodium percarbonate for highly effective degradation of organic compound in aqueous solution. J Ind Eng Chem 68:406–415. https://doi.org/10.1016/j.jiec.2018.08.016

Shao S, Hu Y, Cheng J, Chen Y (2019) Effects of carbon source, nitrogen source, and natural algal powder-derived carbon source on biodegradation of tetracycline (TEC). Bioresour Technol 288:121567

Shi XG, Tian A, You JH, Yu ZQ, Yang H, Xue XX (2016) Fe_2SiS_4 nanoparticle – a new heterogeneous Fenton reagent. Mater Lett 169:153–156. https://doi.org/10.1016/j.matlet.2016.01.073

Shi XG, Tian A, You JH, Yang H, Wang YZ, Xue XX (2018) Degradation of organic dyes by a new heterogeneous Fenton reagent-Fe_2GeS_4 nanoparticle. J Hazard Mater 353:182–189. https://doi.org/10.1016/j.jhazmat.2018.04.018

Stock N, Biswas S (2012) Synthesis of metal-organic frameworks (MOFs): routes to various MOF topologies, morphologies, and composites. Chem Rev 112:933–969

Tibbetts I, Kostakis GE (2020) Recent bio-advances in metal-organic frameworks. Molecules 25:1291

Wang Y, Zhang H, Zhang J, Lu C, Huang Q, Wu J, Liu F (2011) Degradation of tetracycline in aqueous media by ozonation in an internal loop-lift reactor. J Hazard Mater 192:35–43

Wang D, Li J, Xu Z, Zhu Y, Chen G (2019) Preparation of novel flower-like $BiVO_4/Bi_2Ti_2O_7/Fe_3O_4$ for simultaneous removal of tetracycline and Cu(2+): adsorption and photocatalytic mechanisms. J Colloid Interface Sci 533:344–357

Wang Q, Hamilton PB, Kang F, Zhu X, Zhang Y, Zhao H (2020) Regional-scale investigation for microbial competition-through-environment interactions modulating antibiotic resistance. Sci Total Environ 734:139341

Weng X, Owens G, Chen Z (2020) Synergetic adsorption and Fenton-like oxidation for simultaneous removal of ofloxacin and enrofloxacin using green synthesized Fe NPs. Chem Eng J 382:1–11

Wu Z, Wang Y, Xiong Z, Ao Z, Pu S, Yao G, Lai B (2020) Core-shell magnetic Fe_3O_4@Zn/Co-ZIFs to activate peroxymonosulfate for highly efficient degradation of carbamazepine. Appl Catal B 277:119136

Xiao R, Abdu HI, Wei L, Wang T, Huo S, Chen J, Lu X (2020) Fabrication of magnetic trimetallic metal-organic frameworks for the rapid removal of tetracycline from water. Analyst 145:2398–2404

Zhao Z, Zhang G, Zhang Y, Dou M, Li Y (2020) Fe_3O_4 accelerates tetracycline degradation during anaerobic digestion: synergistic role of adsorption and microbial metabolism. Water Res 185:116225

Zhou Y, Zhang Y, Hu X (2020) Novel zero-valent Co–Fe encapsulated in nitrogen-doped porous carbon nanocomposites derived from $CoFe_2O_4$@ZIF-67 for boosting 4-chlorophenol removal via coupling peroxymonosulfate. J Colloid Interf Sci 575:206–219. https://doi.org/10.1016/j.jcis.2020.04.024